16th ICAAR LISBOA 2020-2022

16th International Conference on
Alkali-Aggregate Reaction in Concrete
Lisboa | LNEC | Portugal | 31 May - 2 June 2022

http://icaar2020-2022.lnec.pt

Feasibility of using the electrical resistivity to measure damage from Alkali-Silica Reaction

Chunyu Qiao[(1)], Gaines Green [(2)], Boris Stein [(3)], David Rothstein[(4)]

(1) DRP, a Twining Company, Boulder, USA, joe@drpcinc.com

(2) DRP, a Twining Company, Boulder, USA, gaines@drpcinc.com

(3) Twining, Inc., Long Beach, USA, bstein@twininginc.com

(4) DRP, a Twining Company, Boulder, USA, petro@drpcinc.com

Abstract

Numerous field and lab-based methods attempt to measure the progression of damage due to alkali-silica reaction (ASR). Field-based methods include crack index mapping and crack growth measurements. Macroscopic laboratory-based studies typically involve residual expansion measurements. Microscopical approaches include the damage rating index (DRI), determining the microcrack index, and characterizing the composition of reaction products associated with ASR.

In this pilot study we explore the feasibility of using electrical resistivity to measure the progression of damage from ASR. Cores extracted from a 55-year-old structure affected by ASR serve as the test specimens in this study. Two sets of cores were exposed to residual expansion tests at 38±2°C and 60±2°C for 6 months. Another core not subjected to accelerated residual expansion testing was used as a control. DRI analysis and bulk resistivity were then measured for each specimen. There is a good linear relationship between the DRI scores, bulk resistivity and expansion. Compared to the control, the residual expansion samples show higher DRI scores, and lower bulk electrical resistivity at the Nick point. This is consistent with cracks and microcracks associated with the progression of ASR increasing both the porosity and connectivity of the pore network. The linear relationships between bulk electrical resistivity, DRI scores and residual expansion indicates that bulk electrical resistivity is a useful tool for measuring damage in concrete affected by ASR. This may also be an important initial step to developing techniques to measure how ASR affects concrete transport properties and developing methods to simulate service life of concrete affected by ASR, particularly in environments where chloride penetration is a concern.

Keywords: *alkali-silica reaction; expansion; damage rating index; bulk electrical resistivity*

1. INTRODUCTION

After Stanton first identified the presence of alkali silica reaction (ASR) [1], it has been globally recognized as one of the main deterioration mechanisms in concrete structures, such as dams, bridges, tunnels, pavements, etc. [2-4].

Although the diagnosis of ASR is relatively straightforward using standard methods, such as petrographic examination per ASTM C856 [3,5], understanding and predicting the progression of damage from ASR remains nascent. As such, developing reliable tools and methods that afford an opportunity to quantitatively measure and then predict how the progression of ASR damages concrete remains a prime challenge to managing structures affected by this mechanism. In addition, relatively little is known about how the progression of damage related to ASR affects important properties related to durability, namely transport properties. For example, cracking due to ASR presents an obvious concern for reinforced concrete structures exposed to chlorides in environments ranging from marine structures to roads and bridges in areas where deicing salts are used.

There are few tools available to monitor how the progression of ASR affects structural properties [6,7], while the transport properties are short of understanding as aforementioned. In particular, it can be difficult to assess the status of transport properties in areas of structures that may be less severely affected than those where map cracking is readily observed in the field. The study by Trejo et al. [8] showed that ASR gel can fill the interfacial transition zone and cracks, which reduces chloride transport in concrete. More work is needed to account for the effect of ASR-induced damage on the ionic and moisture transport in concrete.

Although standard field and laboratory techniques, such as crack mapping, strain gauging and petrographic examination [9,10], are in widespread use and effective for documenting the presence of ASR, their utility is limited in terms of understanding the potential for continued expansion [7] and its downstream effects on resistance to chloride penetration and other phenomenon related to durability. Residual expansion testing and measuring available alkalis are useful in determining if there is the potential for continued reaction and expansion, but they do not provide information on how the progress of the reaction may affect the transport properties of concrete.

Researchers and engineers have been exploring the feasibility of non-destructive testing on detecting damage in concrete affected by ASR. Rivard and Saint-Pierre [7] evaluated the ultrasonic wave velocities, dynamic Young modulus and electrical resistivity of ASR damaged concrete and indicated that the P-wave velocities and static Young modulus correlate best with damage due to ASR. Sargolzahi et al. [11] further showed that ultrasonic pulse velocity (UPV) correlates well with the expansion of ASR affected concrete and the petrographic features by the damage rating index (DRI). Flores et al. [3] pointed out that damage from ASR can significantly decrease the electrical resistivity of concrete.

Electrical resistivity of concrete has been widely used through the formation factor to study transport properties relevant to durability issues, such as corrosion of reinforced concrete and freeze-thaw damage of concrete in cold regions. As an indicator of the porosity and connectivity of the pore network, the formation factor provides a means to extract transport properties, such as chloride diffusion coefficient and water sorptivity, from electrical resistivity measurements [12-15]. Qiao et al. [14] used the formation factor, in conjunction with chloride binding studies, to calculate the chloride diffusion coefficient in concrete that is essential for predicting the service life of concrete pavements. Khanzadeh et al. [12] correlated the formation factor to water absorption, which enables the prediction of sorptivity-based service life modelling for freeze-thaw conditions. The above shows the potential of using electrical resistivity and formation factor to capture the change in pore network due to ASR damage in concrete.

This paper examines the feasibility of using electrical resistivity to monitor the progression of damage due to ASR. This is an early step to using electrical resistivity and formation factor to measure transport properties that may be affected by the progression of ASR. This study stems from a forensic investigation of a still in-service concrete structure that is ~ 55 years old. Multiple cores were extracted and then exposed to residual expansion testing for 6 months. After the residual expansion the cores were subjected to petrographic analysis (specifically the damage rating index) and bulk electrical resistivity measurements. The residual expansion, DRI scores and bulk electrical resistivity of the concrete specimens are correlated to each other in this study.

2. MATERIALS AND EXPERIMENTAL PROCEDURES

2.1 Materials

Eight 95 mm diameter cores were extracted from the walls of an indoor pool in the western USA that has been in service for ~ 55 years. The cores represent the entire thickness of the wall and consist of three components (Figure 2.1): (a) tile (~ 5 mm thick); (b) shotcrete (~ 35 mm thick) and (c) concrete (~ 305 mm thick). While the original concrete mix design was not available, petrographic studies indicate the following regarding the concrete: the binder consists of hydrated ordinary portland cement without supplementary cementitious materials (SCMs). Given the age of the structure and the history of cement production in this region, it is likely that a low alkali cement was not used. The original water-cement ratio (w/c) was not estimated because the cores showed evidence of significant fluid penetration manifested by copious deposits of ettringite and ASR gel. The concrete is air-entrained and contains 4% to 7% total air. The aggregate is a natural gravel with a 25 mm nominal top size. The aggregate is siliceous in composition and consists primarily of granitic rocks and quartzite with a minor amount of rhyolite. Petrographic studies conducted prior to the residual expansion testing indicated that the concrete is subject to ongoing ASR (Figure 2.2(b)-(c)), which is rated at Stage IV-Stage V using the scheme described by Katayama et al [16].

Both ends of the cores were trimmed to obtain cylindrical specimens with a length of ~ 250 mm for residual expansion testing, petrographic examination (mainly damage rating index) and electrical resistivity measurements.

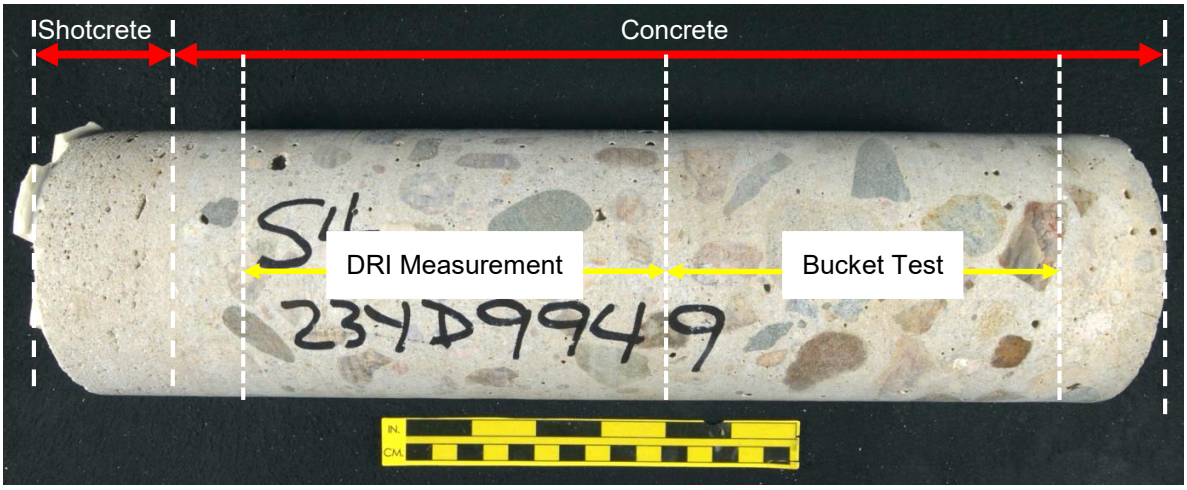

Figure 2.1: Illustration of the core sample used for residual expansion, petrographic and electrical resistivity (bucket test) studies.

2.2 Experimental Procedures

2.2.1 Residual expansion

The residual expansion due to ASR was measured according to a modified procedure of ASTM C1293-18a. The first modification involved the use of cores from an actual structure rather than laboratory-cast concrete prisms made with predetermined aggregate gradations and w/c. The ends of the cores were trimmed with a saw and steel pins were embedded in the ends for length change measurements. The second modification involved placing one set of specimens in sealed reaction vessels kept at 38±2°C per ASTM C1293 while the second set was placed in sealed reaction vessels kept at 60±2°C. The temperature of 60±2°C was chosen according to RILEM recommended test method AAR-4.1.

The initial length of the specimens was measured at 23±2°C and designated as l_0 (mm). The length was measured at 7 days, 14 days, 21 days, 28 days, 56 days, 90 days and 180 days, respectively. Each measurement was done per the standard in a controlled environmental chamber at 23±2°C after the specimens were allowed to equilibrate thermally for 16±4 hrs before taking the length readings, l_t (mm). The relative expansion of the concrete, ε (%), is calculated using the equation below:

$$\varepsilon = \frac{l_t - l_0}{l_0} \times 100\% \quad (1)$$

2.2.2 Damage rating index (DRI)

One specimen from each set of cores was removed from the residual expansion testing after six months. The cores were then cut into two sections, as illustrated in Figure 2.1. One section measuring 120 – 130 mm long was used for petrographic examination. The other section, which measured ~ 100 mm long, was used for the bulk resistivity studies described below. A core extracted from the same wall of the pool as those subjected to the residual expansion was also examined as a control specimen.

The DRI analysis was done following the general procedures described by Sanchez et al.[9,10] using features and weighing factors described by Sanchez et al.[9]. The core was sectioned lengthwise to provide a slab, a cross-sectional slice of the core. One side of the slab was lapped and polished to a 3,000 grit (~ 4 μm) using progressively finer wheels with embedded industrial diamonds. The polished slab was divided into a 1 cm × 1 cm grid and examined at 15x magnification using a stereomicroscope, as illustrate in Figure 2.2. The number of counts corresponding to different petrographic features was tabulated and the counts were multiplied by weighing factors listed in Table 2.1. The DRI work was done by the same operator for the three specimens. The score associated with the sum of these factors was normalized to an area of 100 cm^2.

Thin sections were also prepared for observations of ASR damage in the above three samples using a PELCON automatic machine.

Table 2.1: DRI weighing factors of petrographic features due to ASR (adopted from Refence [9])

Petrographic features	Weighing factor
Crack in aggregate particles (CCA)	0.25
Opened crack in aggregate particles (OCA)	2
Crack with ASR gel in aggregate particles (OCAG)	2
Coarse aggregate debonded (CAD)	3
Crack in cement paste (CCP)	3
Crack with ASR gel in cement paste (CCPG)	3
Disaggregate/corroded aggregate particles (DAP)	2

Figure 2.2: (a) Photograph of the polished surface of the control specimen with drawn grid. (b) Photomicrograph of the polished surface showing one DRI in one cell in (a). (c) Photomicrograph showing the detail of ASR gel (green arrows) lining the cracks in one aggregate particle in (b).

2.2.3 Electrical resistivity

Specimens measuring ~ 100 mm long and ~ 95 mm in diameter were submerged in a 18.9 L bucket containing 10 L of a simulated pore solution. The solution is used to minimize alkali leaching [17]. The composition of the simulated pore solution is 0.3 mol/L NaOH and 0.2 mol/L KOH. 20 g $Ca(OH)_2$ was also added into the solution to prevent calcium leaching. The samples were positioned to ensure all surfaces in contact with the liquid. A volume ratio of the sample to storage solution of 1:8 was used, which is large enough to nullify the influence of concrete samples on the composition of the simulated pore solution [18]. The mass change and electrical resistance were periodically measured over 7 days of submersion at 20±1°C.The electrical resistance was measured using a 38 mm spacing Resipod surface resistivity meter with a bulk resistivity module (Proceq USA, Inc.).

The bulk resistivity of the specimen was calculated using the equation below:

$$\rho_B = \frac{\rho_S}{2\pi a} * \frac{\pi r^2}{l} = \frac{r^2}{2al}\rho_S \quad (2)$$

where, ρ_B and ρ_S are the bulk resistivity (Ω·m) and surface resistivity (Ω·m), respectively; *r*, *l* and *a* are the diameter (m) and length (m) of the specimen, and the spacing between the electrodes (m), respectively. ρ_S is the direct reading from the device.

3. RESULT AND DISCUSSIONS

3.1 Residual expansion

The specimens show expansion over 6-month exposure, with a relative length change or expansion of 0.041% (+0.002%/-0.003%) at 38±2ºC and 0.053% (±0.001%) at 60±2°C (Figure 3.1), respectively. These expansions exceed the expansion threshold of 0.04% from ASTM C1293-18a that classifies aggregates as deleteriously reactive.

Two stages of expansion were observed over the 6-month exposure period. There is an initial stage of rapid expansion over the first 28 days when more than 90% of the total expansion occurs, followed by a second stage of significantly slower expansion between 28 days and six months. This suggests that the penetration of external moisture was sufficient to trigger reaction throughout the cores in the first 28 days, which is consistent with petrographic observations described below. The greater expansion at 60±2°C is associated with increased reactivity of reactive silica in aggregate with the alkaline pore solution at higher temperatures [19].

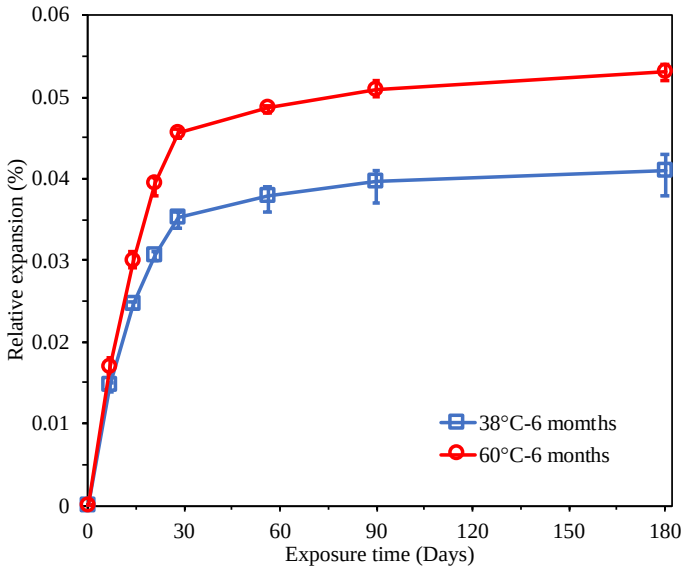

Figure 3.1: Averaged expansion data for specimens exposed to 38±2°C and 60±2°C for 6 months

3.2 Damage rating index

The DRI scores are 89 for the control sample, 289 for the 38±2ºC sample and 318 for the 60±2ºC sample. Figure 3.2 shows the hot maps of the DRI scores in the samples. It indicates that damage increased significantly after the 6-month exposure at elevated temperatures, which is inconsistent with the residual expansion data. Figure 3.2 also indicates the distribution of damage is irregular. While it varies from area to area, damage was observed throughout both of the residual expansion samples. This is consistent with the assumption that the residual expansion test conditions were sufficient to drive ASR throughout the core samples. High DRI scores tend to coincide with areas that contain or are adjacent to reactive aggregate particles.

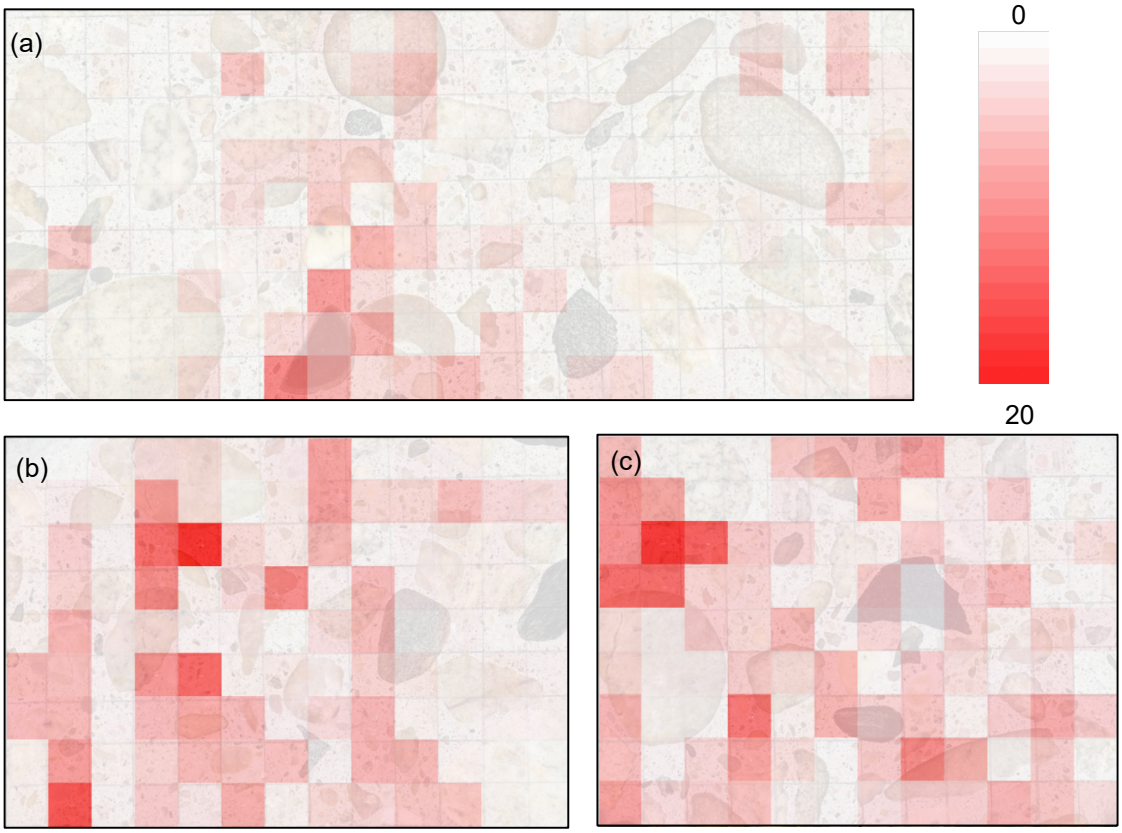

Figure 3.2: The DRI score hot maps of the polished surface of three samples. (a) Control (DRI score = 89); (b) 38±2 °C exposure (DRI score = 289); (c) 60±2 °C exposure (DRI score = 318).

Figure 3.3 shows the DRI scores in different specimens. After elevated temperature exposure for 6 months, more closed cracks in coarse aggregate (CCA) are present because the alkali hydroxide in pore solution entered the originally present cracks in aggregate to react with active silica components to form more cracks with the aggregate particles. As the ASR proceeds, cracks develop and evolve to form more open cracks (OCA+OCAG). Moreover, the open cracks extend into the paste to form more cracks in the paste (CCP+CCPG). In the specimen after 6-month exposure at 60±2°C, more aggregate debonding (CAD) was observed, which may be due to greater expansion in the specimen.

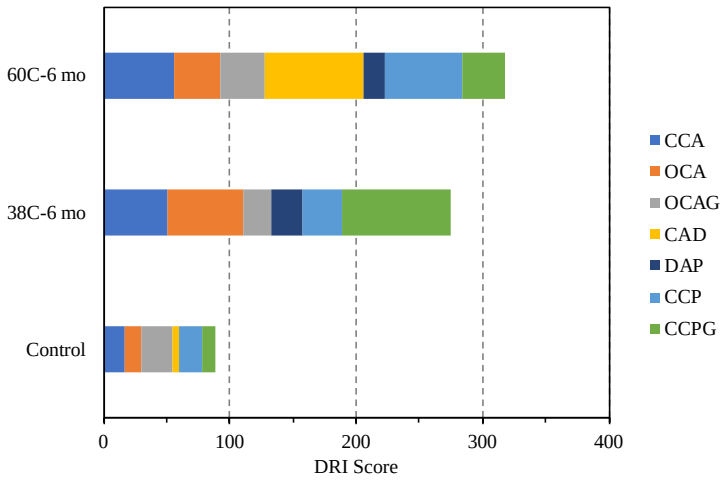

Figure 3.3: Comparison of DRI scores among the samples.

Figure 3.3: (a)-(b) show deposits of ASR gel in microcracks in the control sample and the sample after exposed to 60±2 °C for 6 months. Compared to that in the control sample (in Figure 3.4(c)), the morphology of the freshly formed ASR gel shows fine grains of relatively crystalline particles (in Figure 3.4d). The photomicrographs under fluorescent light (Figure 3.4(e)-(f)) show that the ASR gel in the control sample is relatively dense, while the ASR gel is more porous in the sample after the elevated temperature. This more porous microstructure be due to the that the freshly formed ASR gel exposure tends to absorb water under the high RH during the elevated temperature exposure.

Figure 3.5 shows a good linear relationship between the DRI score and expansion of the concrete specimen. This indicates the feasibility of using DRI to characterize the damage and expansion due to ASR. This is in accordance with the observations by Sanchez et al. [9,10].

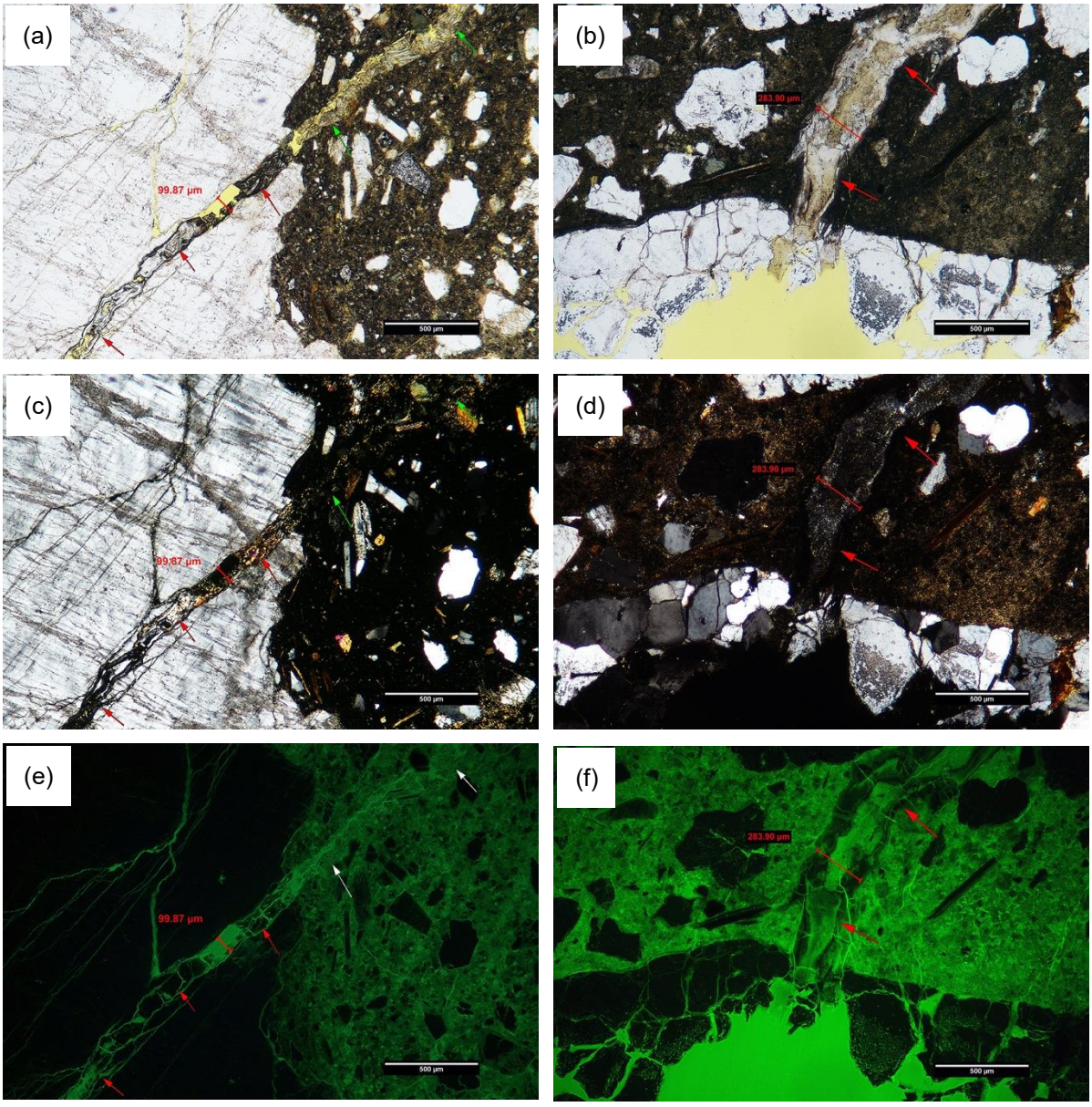

Figure 3.4: Transmitted light photomicrographs of the thin section of the control sample showing ASR gel in a microcrack (red arrows) under (a) plain-polarized light, (c) cross-polarized light and (e) fluorescent light. Transmitted light photomicrographs of the thin section of the sample post-exposure to 60±2 °C showing ASR gel in a microcrack (red/green arrows) under (a) plain-polarized light, (c) cross-polarized light and (e) fluorescent light.

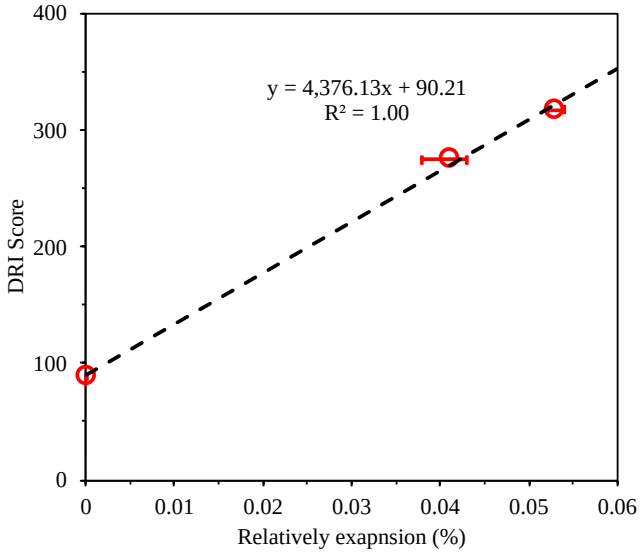

Figure 3.5: The relationship between the relative expansion and DRI scores.

3.3 Bulk electrical resistivity

Figure 3.6(a) shows the change in mass and bulk electrical resistivity over time during the bucket test. As the submersion time increases, more water is absorbed which drives the mass gain. Since more fluid is present to conduct electricity in the pore network of the concrete specimens, the electrical resistivity drops over time until it reaches a steady state value.

As shown in Figure 3.6(a), the water absorption into the concrete specimen follows two linear stages as functions of square root of time. This is similar to the observations in previous studies [13,15]. Since all the matrix pores (capillary pore and gel pores) tend to rapidly fill with fluid due to capillary suction, the mass gain is rapid in the first couple of days (Figure 3.6(a)). After all the matrix pores are filled, the air voids in the concrete begin to fill due to moisture diffusion, which is a slower process that takes months to years [15,20].

Qiao et al. [15] showed that concrete specimens (w/c=0.40 – 0.50) with a similar dimension have all the matrix pores filled in the first 5 days during bucket tests, while leaving the majority of the air voids empty. The degree of saturation, at which all the matrix pores are filled and all the air voids are empty, is named the Nick point. Since the mixture proportion remains unknown in this study, 7 days is assumed to be enough for the specimens to reach Nick point and the bulk electrical resistivity at 7 days is considered to be the value at Nick point.

At a given degree of saturation, the electrical resistivity of the concrete is determined by the pore network (porosity and connectivity) and the electrical resistivity of the pore solution [15]. Since the same simulated pore solution was used in the bucket test, the difference in the electrical resistivity of the specimens at Nick point (at 7 days) will mainly reflect the change in matrix pore network, both in porosity and connectivity.

Figure 3.6(b) compares the electrical resistivity in the specimens with and without exposure at elevated temperatures for 6 months. The residual expansion samples show a lower bulk electrical resistivity than the control. This is consistent with the cracks as observed in the DRI analysis increasing the porosity and connectivity of the matrix pore network. More open cracks were observed in the specimen exposed to 60±2°C (in Figure 3.5), which has a lower electrical resistivity than the 38 ±2ºC sample.

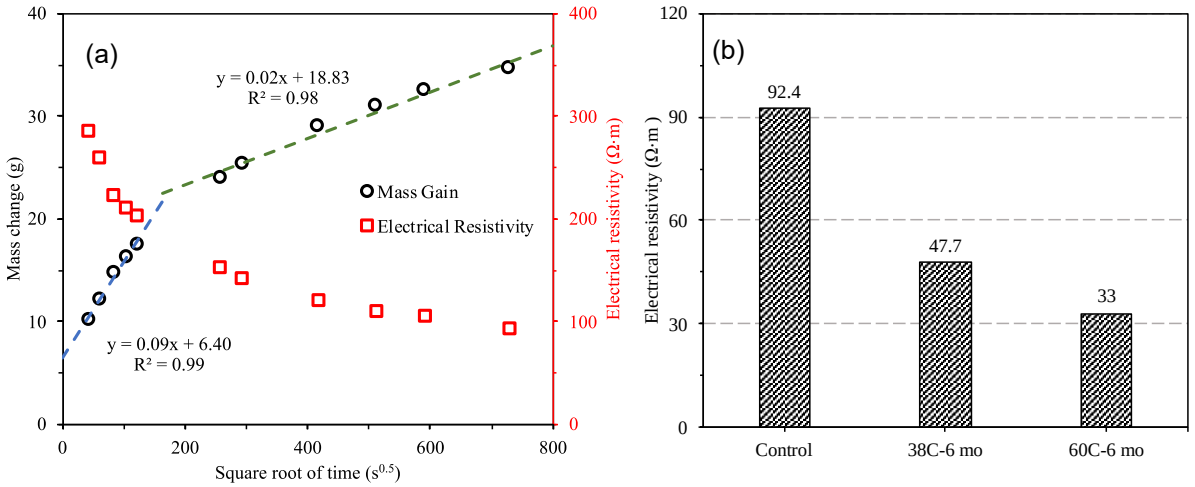

Figure 3.6: (a) The change in mass and electrical resistivity of the control sample as functions of time during bucket test. (b) The comparison of bulk electrical resistivity of three samples after 7 days.

3.4 Relationship between electrical resistivity and ASR damage

The measurements of residual expansion, DRI score and bulk electrical resisivity are all associated with cracking and damage due to ASR. Figure 3.7 correlates the electrical resistivity to the residual expansion and the DRI scores. Figure 3.7 indicates that the bulk electrical resistivity shows linear relationships with the DRI scores and the residual expansion. This data suggests that bulk resistivity is a useful tool to measure the progression of damage in ASR affected concrete.

Measurement of bulk electrical resisivity shows several promising features for measuring damage. Compared to DRI, the electrical resisivity measurement is less time-consuming and more objective, as it eliminates operator bias. Bulk resistivity may also be more sensitive to monitoring how microcracks, which may well be overlooked at the relatively low magnification used in DRI analyses, cause damage. More information regarding how the progresson of damage affects durability can be extracted from bulk electrical resistivity. The formation factor could be calcuated from bulk electrical resisivity by knowing the electrical resistivity of the pore solution. Furthermore, the formation factor can be used to predict the chloride and mositure transport in concrete [12,14], which are critical to corrosion and freeze-thaw damage, respectively. As such, there is promise in using bulk electrical resistivity as a tool to study the effects of ASR on service life associated with chloride-induced corrosion and freeze-thaw damage in cold regions. However, more work is neccessary to clarify the effect of ASR on the pore solution chemistry as the reaction proceeds because the accuracy of the formation factor calculation strongly relies on the electrical resistivity of the actual pore solution.

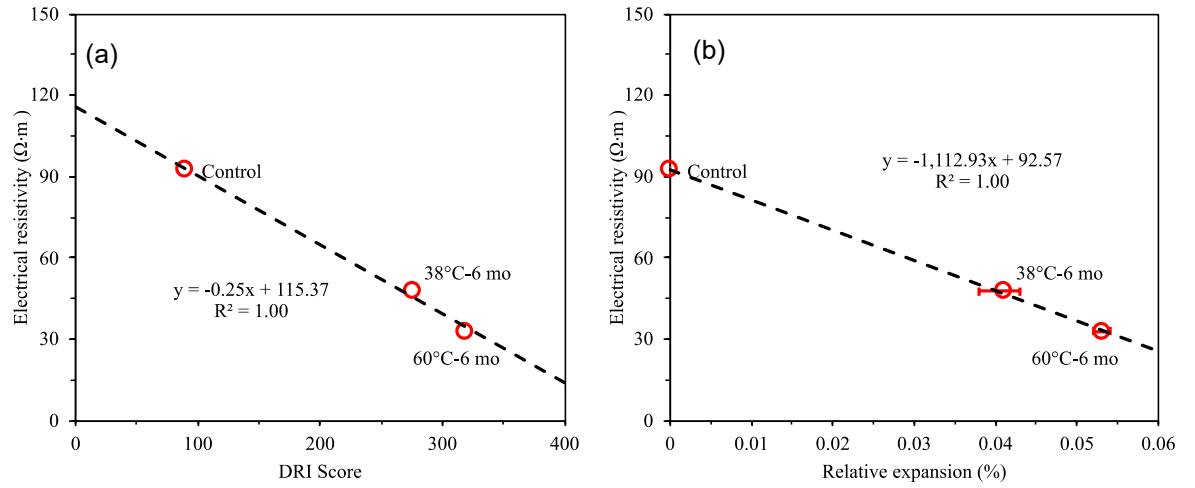

Figure 3.7: (a) The relationship between the bulk electrical resistivity and the expansion rate of the samples. (b) The relationship between the electrical resistivity and the DRI scores of the samples.

4. CONCLUSIONS

This paper reports the residual expansion, DRI scores and bulk electrical resistivity of cores extracted from a 55-year old concrete structure after exposure to elevated T/RH conditions (38±2°C and 60±2°C/100% RH) for 6 months. DRI and bulk electrical resistivity measurements were also measured in a core from the same structure that was not subjected to residual expansion testing.

The residual expansion of the specimens after a 6-month exposure time exceed the 365-day length expansion threshold of 0.04% from ASTM C1293-18a that is used to classify aggregates as deleteriously reactive. A greater expansion was observed in the specimen exposed to higher temperature. Similarly, the DRI score increased in specimens after the elevated temperature exposure and a higher DRI score was obtained in the specimen exposed to higher temperature. There is a good linear relationship between the DRI scores and expansion.

Compared to the control, the residual expansion specimens show lower bulk electrical resistivity at the Nick point. This data correlates with open cracks in aggregate particles and the cement paste increasing the connectivity of the matrix pore network. The bulk electrical resistivity shows good linear relationships with both DRI scores and expansion of the specimens within this paper. This indicates the feasibility of using bulk electrical resistivity to characterize the damage progress due to ASR and potentially to predict the service life in the ASR-affected concrete structure.

5. ACKNOWLEDGEMENTS

The authors gratefully acknowledge support for this work by Robert Ryan and Edward Twining of Twining Laboratories. The authors thank Robert Davenport and Joe Wnukowski for their assistance with conducting of the experiments and Grace Guryan for her efforts with sample preparation.

6. REFERENCES

[1] Stanton TE (1940) Expansion of Concrete through Reaction between Cement and Aggregate. Proceedings of the ASCE 66 (10):1781-1811

[2] Ono K (1988) Damaged concrete structures in Japan due to alkali silica reaction. International Journal of Cement Composites and Lightweight Concrete 10 (4):247-257. https://doi.org/10.1016/0262-5075(88)90055-3

[3] Rivard P, Ballivy G, Gravel C, Saint-Pierre F (2010) Monitoring of an hydraulic structure affected by ASR: A case study. Cement and Concrete Research 40 (4):676-680. https://doi.org/10.1016/j.cemconres.2009.09.010

[4] Thomas E. Stanton OJPLCM, Allen N (1942) California Experience With the Expansion of Concrete Through Reaction Between Cement and Aggregate. ACI Journal Proceedings 38:209-236. https://doi.org/10.14359/8598

[5] Kerrick DM, Hooton RD (1992) ASR of concrete aggregate quarried from a fault zone: Results and petrographic interpretation of accelerated mortar bar tests. Cement and Concrete Research 22 (5):949-960. https://doi.org/10.1016/0008-8846(92)90119-G

[6] Omikrine Metalssi O, Godart B, Toutlemonde F (2015) Effectiveness of nondestructive methods for the Evaluation of structures affected by internal swelling reactions: a review of electric, seismic and acoustic methods based on laboratory and site experiences. Experimental Techniques 39 (2):65-76. https://doi.org/10.1111/ext.12010

[7] Rivard P, Saint-Pierre F (2009) Assessing alkali-silica reaction damage to concrete with non-destructive methods: From the lab to the field. Construction and Building Materials 23 (2):902-909. https://doi.org/10.1016/j.conbuildmat.2008.04.013

[8] Trejo D, Mazarei V, Ideker JH, Isgor OB (2017) Influence of Alkali-Silica Reaction Reactivity on Corrosion in Reinforced Concrete. ACI Materials Journal 114 (5):723-731. https://doi.org/10.14359/51689895

[9] Sanchez LFM, Fournier B, Jolin M, Bedoya MAB, Bastien J, Duchesne J (2016) Use of Damage Rating Index to Quantify Alkali-Silica Reaction Damage in Concrete: Fine versus Coarse Aggregate. ACI Materials Journal 113 (4):395-407. https://doi.org/10.14359/51688983

[10] Sanchez LFM, Fournier B, Jolin M, Duchesne J (2015) Reliable quantification of AAR damage through assessment of the Damage Rating Index (DRI). Cement and Concrete Research 67:74-92. https://doi.org/10.1016/j.cemconres.2014.08.002

[11] Sargolzahi M, Kodjo SA, Rivard P, Rhazi J (2010) Effectiveness of nondestructive testing for the evaluation of alkali–silica reaction in concrete. Construction and Building Materials 24 (8):1398-1403. https://doi.org/10.1016/j.conbuildmat.2010.01.018

[12] Moradllo MK, Qiao C, Isgor B, Reese S, Weiss WJ (2018) Relating the formation factor of concrete to water absorption. ACI Materials Journal 115 (6):887-898

[13] Moradllo MK, Qiao C, Keys M, Hall H, Ley MT, Reese S, Weiss WJ (2019) Quantifying Fluid Absorption in Air-Entrained Concrete Using Neutron Radiography. ACI Materials Journal 116 (6). https://doi.org/10.14359/51716980

[14] Qiao C, Coyle A, Isgor B, Weiss J (2018) Prediction of Chloride Ingress in Saturated Concrete Using Formation Factor and Chloride Binding Isotherm. Advances in Civil Engineering Materials 7 (1):206-220. https://doi.org/10.1520/ACEM20170141

[15] Qiao C, Moradllo MK, Hall H, Ley MT, Weiss WJ (2019) Electrical Resistivity and Formation Factor of Air-Entrained Concrete. ACI Materials Journal 116 (3):85-93. https://doi.org/10.14359/51714506

[16] Katayama T, Tagami M, Sarai Y, Izumi S, Hira T (2004) Alkali-aggregate reaction under the influence of deicing salts in the Hokuriku district, Japan. Materials Characterization 53 (2):105-122. https://doi.org/10.1016/j.matchar.2004.07.003

[17] Spragg R, Bu Y, Snyder KA, Bentz DP, Weiss J (2013) Electrical testing of cement-based materials: Role of testing techniques, sample conditioning, and accelerated curing. Joint Transportation Research Program. https://books.google.com/books?id=FUOWoAEACAAJ

[18] Todak HN (2015) Durability assessments of concrete using electrical properties and acoustic emission testing. Purdue University, West Lafayette

[19] Ulm F-J, Coussy O, Kefei L, Larive C (2000) Thermo-Chemo-Mechanics of ASR Expansion in Concrete Structures. Journal of Engineering Mechanics 126 (3):233-242. https://doi.org/10.1061/(ASCE)0733-9399(2000)126:3(233)

[20] Todak H, Lucero CL, Weiss WJ (2015) Why is the Air There? Thinking about Freeze-Thaw in Terms of Saturation. Concrete Infocus. NRMCA